Composites: Part A 153 (2022) 106727

Contents lists available at ScienceDirect

Composites Part A

journal homepage: www.elsevier.com/locate/compositesa

# Flexible polyvinylidene fluoride(PVDF)/MXene($Ti_3C_2Tx$)/Polyimide(PI) wearable electronic for body Monitoring, thermotherapy and electromagnetic interference shielding

Min Sang [a,b], Shuai Liu [a], Wenwen Li [a], Sheng Wang [a], Jun Li [b], Ji Li [b], Shouhu Xuan [a,*], Xinglong Gong [a,*]

[a] CAS Key Laboratory of Mechanical Behavior and Design of Materials, Department of Modern Mechanics, University of Science and Technology of China, Hefei, Anhui 230027, China

[b] Anhui Weiwei Rubber Parts Group Co. Ltd., Tongcheng, Anhui, 231460, China

ARTICLE INFO

*Keywords:*
A. Multifunctional composites
A. Sandwich structures
B. Electrical properties
Wearable electronic

ABSTRACT

Recently, multifunctional materials have attracted tremendous attention in intelligent equipment and human–computer interaction, requiring the integration of electrical conductivity, sensing property and heating management. Herein, conductive MXene is formulated and deposited on the PVDF film surface and followed by integrating PI tape to construct a multifunctional PVDF/MXene/PI wearable electronic. The PVDF/MXene/PI with sandwich structure shows ideal mechanical strength and tensile toughness. Based on the conductive MXene network, PVDF/MXene/PI composite possesses excellent mechanosensation ability, which can sensitively monitor different human movements. Besides, PVDF/MXene/PI composite presents prominent Joule heating capability and achieves a temperature of over 80 ℃ at 6.5 V voltage. Insulated high-temperature resistant PVDF and PI tape as protective layers ensure the stability and safety of PVDF/MXene/PI heater. Moreover, PVDF/MXene/PI composite exhibits outstanding electromagnetic interference shielding effectiveness of 40 dB. Finally, PVDF/MXene/PI multifunctional electronic with fascinating multi-functions shows potential applications in human thermotherapy, human–machine interaction and electromagnetic wave protection.

## 1. Introduction

With the development of information technology and artificial intelligence, smart wearable electronic products show promising prospects in man–machine interaction [1-5]. As a group of smart devices in the new era, wearable smart electronic devices are developing rapidly to realize functions such as human motion sensing and personal health monitoring [6-8]. In addition, the popularization and development of smart electronic devices has aggravated another serious problem, namely the electromagnetic waves radiated by these electronic devices [9]. Electromagnetic radiation not only negatively affects the performance of some precision instruments, but also seriously hurts human health, causing nausea, headaches and cancers [10]. Therefore, it is of great application value to design and develop smart wearable electronic with electromagnetic shielding performance, so as to protect the human body and precision electronic devices from electromagnetic radiation, and meanwhile possess the ability to respond to different environmental stimuli. At present, numerous studies have reported multifunctional electronic devices with electromagnetic interference shielding capabilities, greatly expanding the application range of traditional wearable electronic devices [11-13].

At the same time, human survival has to cope with the impact of different climatic environments. Under cold conditions, the heat emitted by human itself can only maintain the basic survival. In this case, electrical heaters have aroused great research interest, which exhibit prospects in the fields of intelligent heating equipment, thermotherapy and food thermal processing [14-16]. Furthermore, if the wearable electronic is given a heating function, it can provide energy for the human body in a cold environment, prevent the human body from being attacked by colds and diseases, thus provide a comprehensive protection system for the human body. However, for current wearable electronic, the integration of electromagnetic shielding, electrothermal therapy, and human motion detection is still a huge challenge, which cannot meet the requirements for the versatility of materials in complex

* Corresponding authors.
*E-mail addresses:* xuansh@ustc.edu.cn (S. Xuan), gongxl@ustc.edu.cn (X. Gong).

https://doi.org/10.1016/j.compositesa.2021.106727
Received 27 July 2021; Received in revised form 10 November 2021; Accepted 17 November 2021
Available online 20 November 2021

environments, especially in some specific scenarios. Recently, MXene as a typical two-dimensional (2D) inorganic conductive materials which possesses excellent electrical conductivity exhibits promising applications in electromagnetic shielding [17,18], wearable electronic [19,20] and electronic heater [21,22]. The surface terminations (–OH, -O, and -F) enable MXenes to be dispersible in solvents, thus can be solution-manufactured through various coating techniques such as spin-casting and spray-coating [23,24]. Zhang and co-workers [25] developed a highly stretchable, conductive and hierarchical polydimethylsiloxane (PDMS)/$Ti_3C_2Tx$ MXene films for efficient electromagnetic interference shielding and pressure sensing. Wang et al. [26] reported a multifunctional polymeric textile-based wearable heater decorated with MXenes on a fiber surface. The MXene-decorated textiles exhibit exceptional electrothermal heating performance with a wide temperature range of 40–174 ℃ under 1–3.5 V. However, pure MXene usually possesses poor mechanical strength, such as MXene film [27] and MXene aerogels [28]. In this case, MXene/polymer composites are expected to show numerous advantages, such as good flexibility, ideal mechanical properties and versatile functions.

Here in, this work reports a multifunctional PVDF/MXene/PI wearable electronic sensor with electromagnetic shielding ability and electric therapy performance via spray-depositing MXene nanosheeets on the PVDF surface and then pasting insulating PI tape. By assembling three-layer structure, PVDF/MXene/PI possesses ideal mechanical properties. The prepared PVDF/MXene/PI wearable electronic exhibits obvious resistance changes under the loading of different external strains, which is caused by the microscopic changes of the MXene conductive layer during the bending process. Based on its strain sensing performance, PVDF/MXene/PI wearable electronic can be further attached to the human body to monitor and distinguish different human movements. Besides, PVDF/MXene/PI wearable electronic generates Joule heat under the stimulus of voltage, thus can supply warmth or electric therapy to the human body under cold external conditions. More importantly, PVDF/MXene/PI wearable electronic also exhibits prominent electromagnetic shielding performance, which can protect the human body from electromagnetic radiation. Based on the above functions, PVDF/MXene/PI wearable electronic provides a comprehensive protection for the human body and is expected to become a new generation of multifunctional wearable electronic devices.

## 2. Material and experiments

### 2.1. Materials

Poly(vinylidene fluoride) (PVDF) particles were provided by Sigma-Aldrich. *N*-methyl pyrrolidone (NMP) solvent and lithium fluride (LiF) were purchased from Aladdin Chemical Co., Ltd, Shanghai, China. $Ti_3AlC_2$ MAX precursor was provided by 11 Technology Co., Ltd, Jilin, China. Hydrochloric acid (HCl) was bought from Sinopharm Chemical Reagent Co., Ltd, Shanghai, China. The polyimide (PI) tape was commercially available products. All above chemical reagents were employed without further purification and distilled water was used.

### 2.2. Synthesis of delaminated MXene nanosheets

MXene nanosheets was synthesized by etching $Ti_3AlC_2$ precursor using LiF/HCl solution to selectively eliminate Al layer (Fig. 1). First, 2 g of $Ti_3AlC_2$ powder was slowly added into 40 mL HCl (9 M) containing 2 g of LiF in a Teflon beaker. After reacting at 35 ℃ for 24 h, the obtained product was washed with deionized water and centrifuged several times until the pH of supernatant exceed 6. Afterwards, the above sediment was dispersed in deionized water and followed by ultrasound to

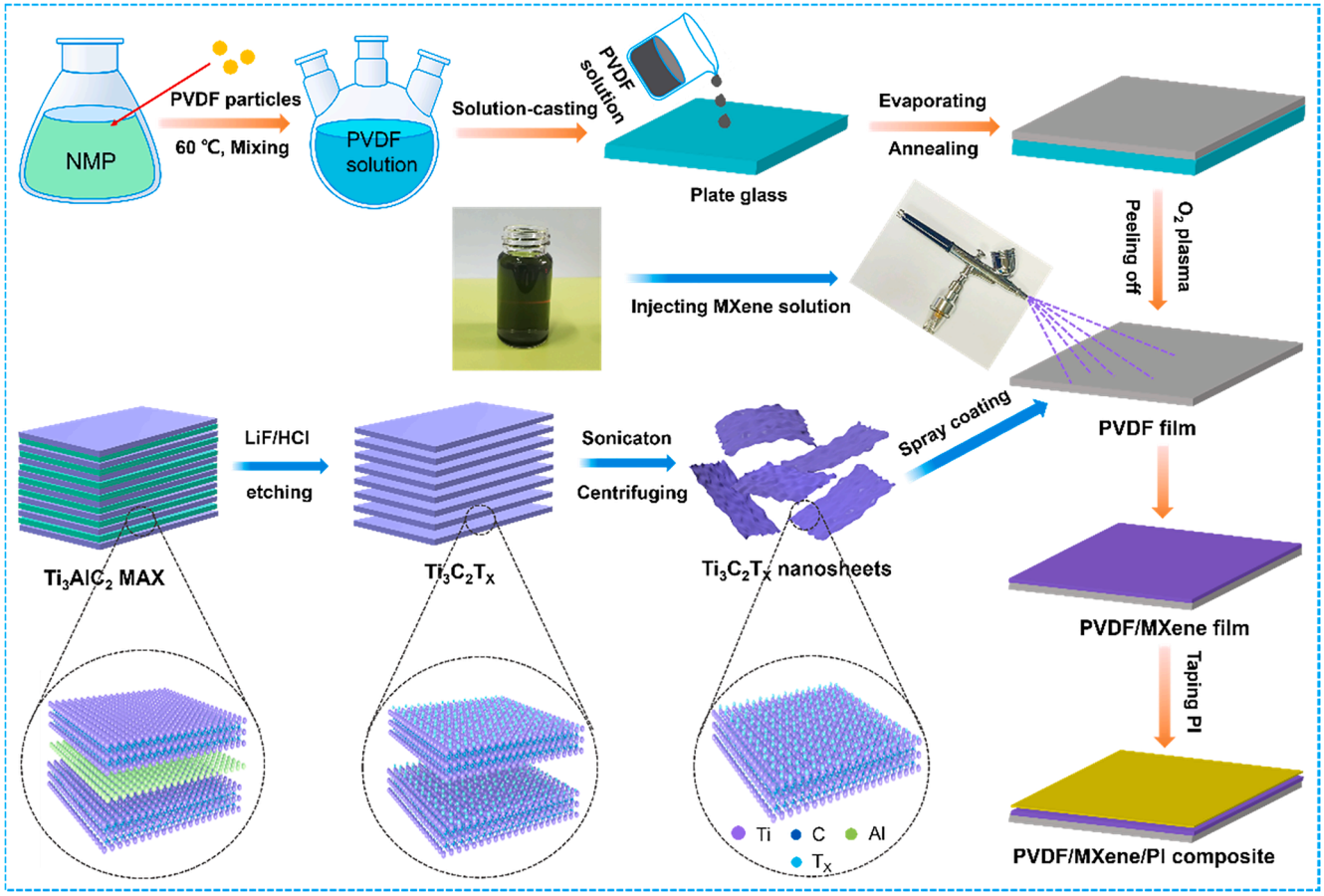


**Fig. 1.** The schematic diagram showing the fabrication process of MXene nanosheets and PVDF/MXene/PI composite.

exfoliate multilayer MXene. Centrifuging at 3500 rpm for 1 h, the delaminated MXene nanosheets were collected and a concentrated $Ti_3C_2T_X$ colloidal dispersion was finally obtained.

### 2.3. Fabrication of PVDF/MXene/PI composite structure

Briefly, PVDF film was firstly synthesized by a solution-casting method [29]. 10.6 g of PVDF particles were dissolved in 60 mL of NMP solvent at 60 ℃ for 2 h to get PVDF solution (15 wt%). Afterwards, the above PVDF solution was casted onto a clean and horizontal glass plate, evaporated at 60 ℃ for 12 h and annealed at 120 ℃ for 8 h to obtain PVDF free-standing film. To fabricate the PVDF/MXene/PI composite structure, PVDF film was soaked in ethanol solution for 20 min and dried in the oven to clean the impurities on the surface. In order to improve the interface interaction between MXene nanosheets and PVDF film, the cleaned PVDF film was treated by an $O_2$ plasma vapor deposition equipment as hydrophilic modification for 50 s (50 W), where $O_2$ was used as etching gas. Then, $Ti_3C_2Tx$ MXene nanosheets were spraying-coated on the surface of modified PVDF film as conductive active materials under 2 bar air pressure by using a spray gun with an aperture of 0.5 mm and dried on a heating stage. Since the self-adhesive PI tape has a sticky layer, thus can be attached directly to the PVDF/$Ti_3C_2Tx$ surface to finally obtain PVDF/MXene/PI composite structure (Fig. 1). For simplicity, PVDF/MXene/PI composite structures with different MXene contents are defined as PVDF/XMXene/PI, where X is the loading density (mg/cm$^2$) of MXene. Here, the loading density of MXene was determined by weighing the added mass sprayed on the fixed area of the PVDF film.

### 2.4. Characterization

The surface and the cross-sectional morphology images were characterized by scanning electron microscopy (SEM, Sirion 200). The transmission electron microscopy morphology was characterized by field-emission transmission electron microscopy (FETEM, JEM-2100F). The atomic force microscope (AFM, dimension icon, Bruker) was employed to record the height morphology of MXene nanosheets. An X-ray diffractometer (XRD, SmartLab, Japan) was used to characterize the crystalline phase of $Ti_3AlC_2$ MAX and MXene nanosheets. The X-ray photoelectron spectum (XPS) were characterized by a Thermo ESCALAB250Xi spectrometer. The Materials Test System (MTS) (ASTM D-882) was used to test the mechanical properties of samples. The electrical conductivity of PVDF/MXene film was tested by the standard four-point contact method (FT-340, Ningbo rooko instrument Co., Ltd., China). The electromagnetic interference shielding values were tested by ASTM D 4935–89 using a vector network analyzer (AV3672, China electronics technology instruments Co., Ltd). The electrical sensing properties were measured by the ModuLab materials test system (Solartron analytical, AMETEK advanced measurement technology, Inc., United Kingdom). The applied bending strain and displacement were controlled by the dynamic mechanical analyzer (DMA, ElectroForce 3200, TA instruments, Minnesota 55,344 USA). The Joule heating performance was investigated by a DC power supply (IT8500, Itech electronic Co., Ltd) and a thermocouple device (DT-3891G, Shenzhen Everbest Machinery Industry Co., Ltd, China). An infrared camera (ImageIR 8325) was used to record infrared electrothermal images.

## 3. Results and discussion

### 3.1. Characterization of MXene nanosheets and PVDF/MXene/PI composite structure

In order to prove the successful etching of $Ti_3AlC_2$ precursor, XRD and XPS characterization were carried out. The strong peak (1 0 4) at 39°of $Ti_3AlC_2$ vanishes, indicating that the Al layer is completely eliminated (Fig. 2a). In addition, the representative peak (0 0 2) (9.3°) moves to a lower angle (6.2°), suggesting that the layer spacing of MXene increases after etching and stripping. The XPS test results show the binding energy of Ti 2p, Al 2p, O 1 s and C 1 s, the Al 2p peak disappears obviously after etching, further demonstrating the Al layer is completely removed (Fig. 2b and c). Fig. 2d shows the TEM image of MXene nanosheets. The etched and delaminated MXene nanosheets present a

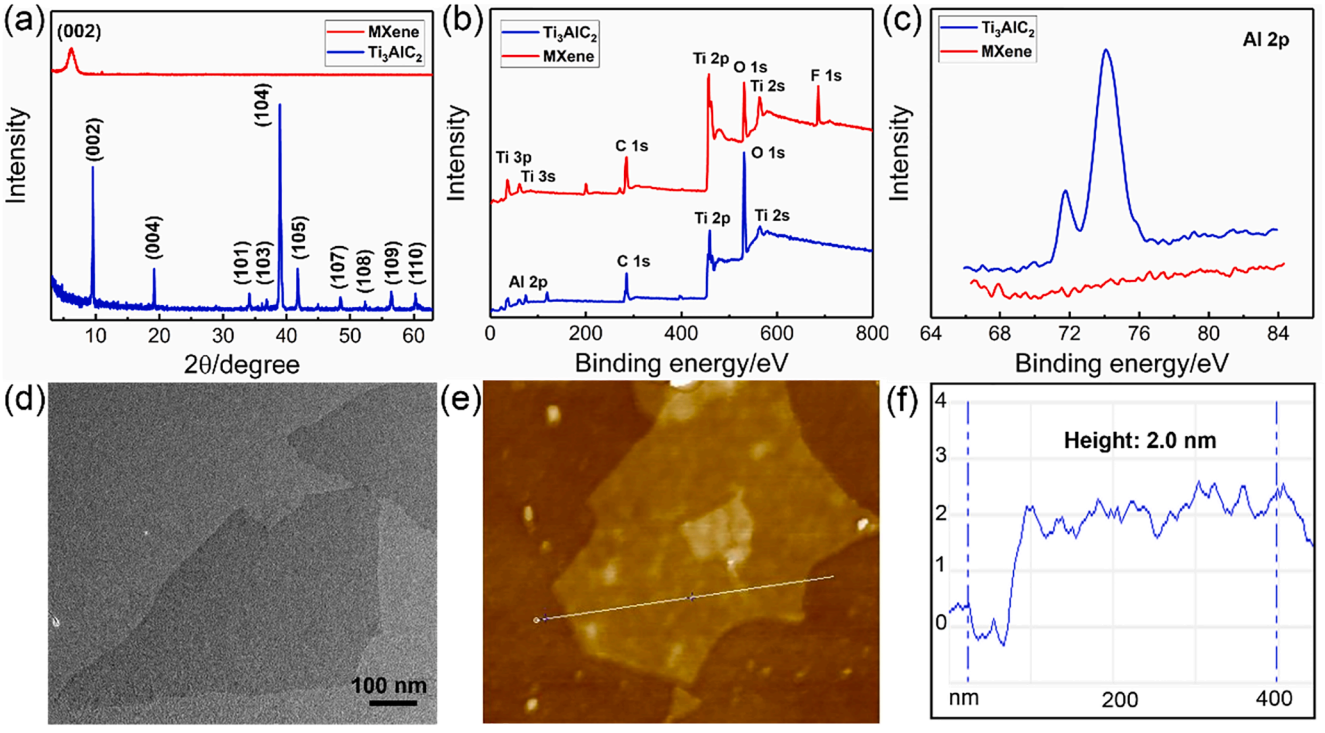


**Fig. 2.** (a) XRD pattern and (b, c) XPS spectrum of $Ti_3AlC_2$ precursor and MXene nanosheets. (d) TEM image and (e, f) AFM morphology of delaminated MXene nanosheets.

thin and transparent lamellar structure. In accordance with TEM characterization result, AFM morphology also shows the lamellar structure of MXene nanosheets (Fig. 2e). Additionally, the AFM height topography shows the thickness of the synthesized MXene nanosheets of about 2.0 nm, which highly proves the successful synthesis of single-layer/few-layer MXene nanosheets (Fig. 2f).

SEM is used to characterize the surface and interface morphologies of PVDF/MXene/PI composite. The surface of PVDF film synthesized by solution-casting method presents a spherical cell structure, which is rough and convex (Fig. 3a). After depositing MXene nanosheets, the surface of PVDF/MXene shows a porous network structure morphology (Fig. 3b). The MXene droplets are coated on the surface of PVDF film in the form of emission when the spray gun ejects the MXene solution, thus results in a continuously porous structure on the PVDF/MXene surface. To confirm the $O_2$ plasma sputtering can be employed to modify the surface of PVDF film to improve the interface interaction between MXene nanosheets and PVDF film, the interface change between PVDF and MXene layers of PVDF/MXene composite film without/with $O_2$ plasma sputtering treatment were compared. As shown in Figure S1, it was found that PVDF/MXene composites without $O_2$ plasma sputtering treatment (left) would obviously show delamination and wrinkling phenomenon at high temperature, while PVDF/MXene composites with $O_2$ plasma sputtering treatment would not show delamination phenomenon at high temperature, proving that the interface adhesion between PVDF and MXene layers was obviously improved through $O_2$ plasma sputtering treatment [30,31]. From the cross-section image of PVDF/MXene/PI sandwich structure, the three-layer of PI, MXene and PVDF can be clearly observed (Fig. 3c). The thicknesses of the PI, MXene and PVDF layer are approximately 68, 18 and 35 μm, respectively. The corresponding element mapping images show the spatial distribution of Ti, C, O, N and F elements, which further confirms the distinct three-layer structure of PVDF/MXene/PI (Fig. 3d). To explore the mechanical property of PVDF/MXene/PI sandwich structure, tensile tests were firstly carried out (Fig. 3e). Here, the effective distance between the fixtures as the original length ($L_0$) of the tensile specimen is selected to calculate the elongation in the mechanical test. According to the stress–strain curve, PVDF/MXene/PI sandwich structure exhibits two fracture points (Fig. 3f). The first fracture point is attributed to the tensile failure of PVDF/MXene bilayer, and the second fracture point is derived from the tensile failure of PI layer. Besides, PVDF/MXene breaks at 7.59% tensile strain, showing typical brittle behavior (Figure S2a), while PI shows significant toughness and can withstand large tensile

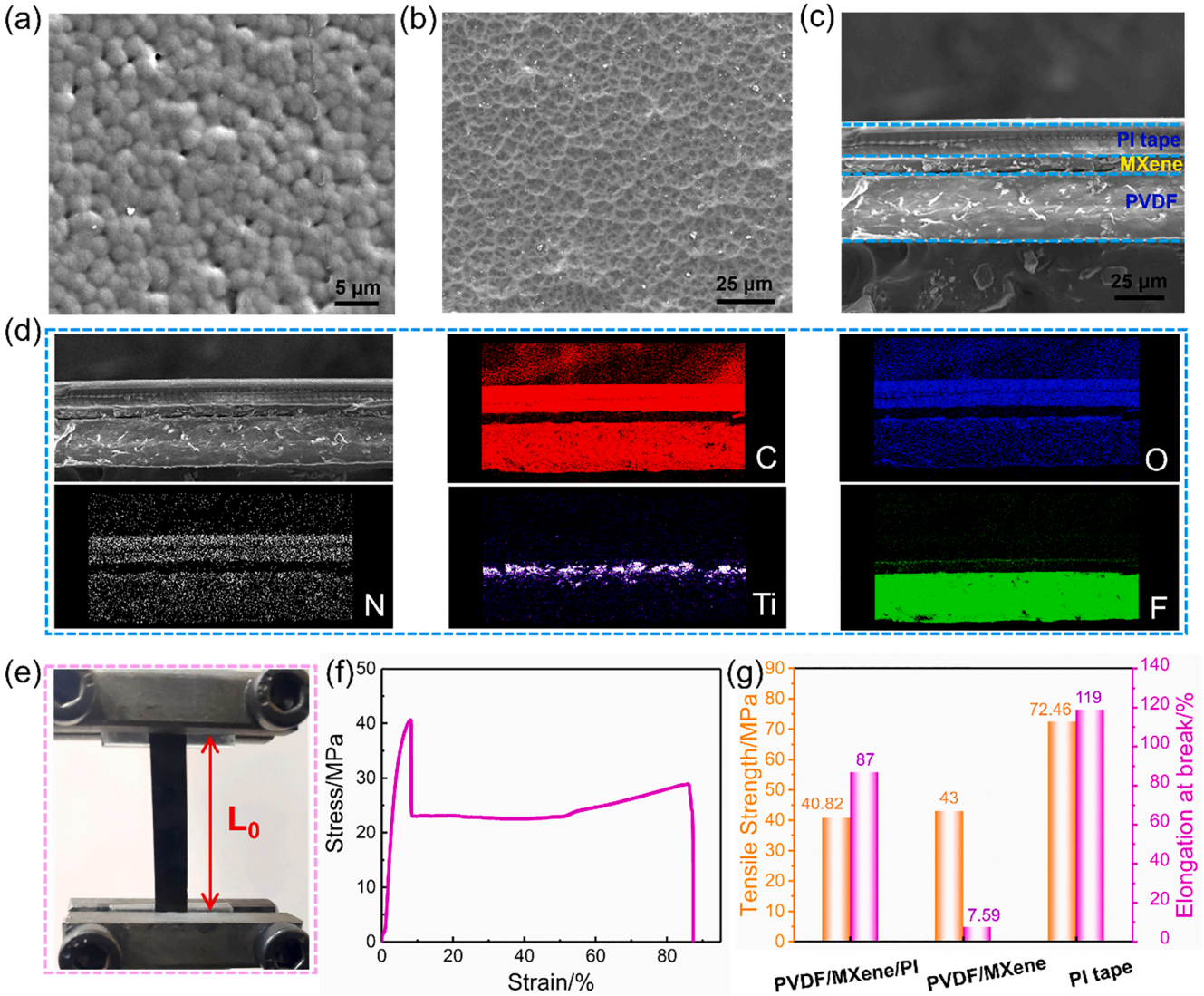


**Fig. 3.** SEM surface images of (a) PVDF film and (b) PVDF/MXene film. (c) The cross-sectional SEM image of PVDF/MXene/PI composite structure and (d) the corresponding elemental mapping image. (e) The diagram of tensile test conducted by MTS measurement. (f) The stress–strain curves of PVDF/MXene/PI composite structure. (g) The tensile strength and elongation of PI tape, PVDF/MXene and PVDF/MXene/PI.

strain with elongation at break of 119% (Figure S2b). By forming three-layer structure, PVDF/MXene/PI composite can maintain good mechanical strength (maximum tensile strength is 40.82 MPa), while being endowed with good toughness (elongation at break is 87%) (Fig. 3g), thus guarantees its durability and universality in practical applications. In order to further explore the interfacial interaction of PVDF/MXene/PI composite structure, the peel force between layers of material by using Dynamic mechanical analysis (DMA) equipment is measured. As shown in Figure S3a and 3b, when the peel displacement is set to 5 mm, the peel force of PVDF/MXene layer and PI layer reaches 2.8 N. Based on the test result and the self-adhesion property of PI, it is not easy to slip and peel off between PVDF/MXene layer and PI layer. More important, it can be seen from Figure S3d that after peeling, the spray-coated MXene nanosheets are still attached to the PVDF film surface, but do not transfer to the PI layer due to the stickness of PI tape, which further indicates that the interface interaction between PVDF and MXene nanosheets can be enhanced by oxygen plasma treatment.

### 3.2. *Mechanical-electrical coupling sensing performance of PVDF/MXene/PI wearable electronic*

To investigate the mechanical–electrical sensing performance, PVDF/MXene/PI wearable electronic were fixed on the DMA fixture. The bending strain was determined by applying different bending displacements. Meanwhile, impedance instrument was used to record the resistance change signal (Fig. 4a). During the loading and unloading cycles of different bending strains, the resistance of the PVDF/MXene/PI wearable electronic produces a real-time resistance change, showing significant stimulus–response characteristics to the external strain. As shown in Fig. 4b, when the bending strain varies from 10%, 15%, 20%,

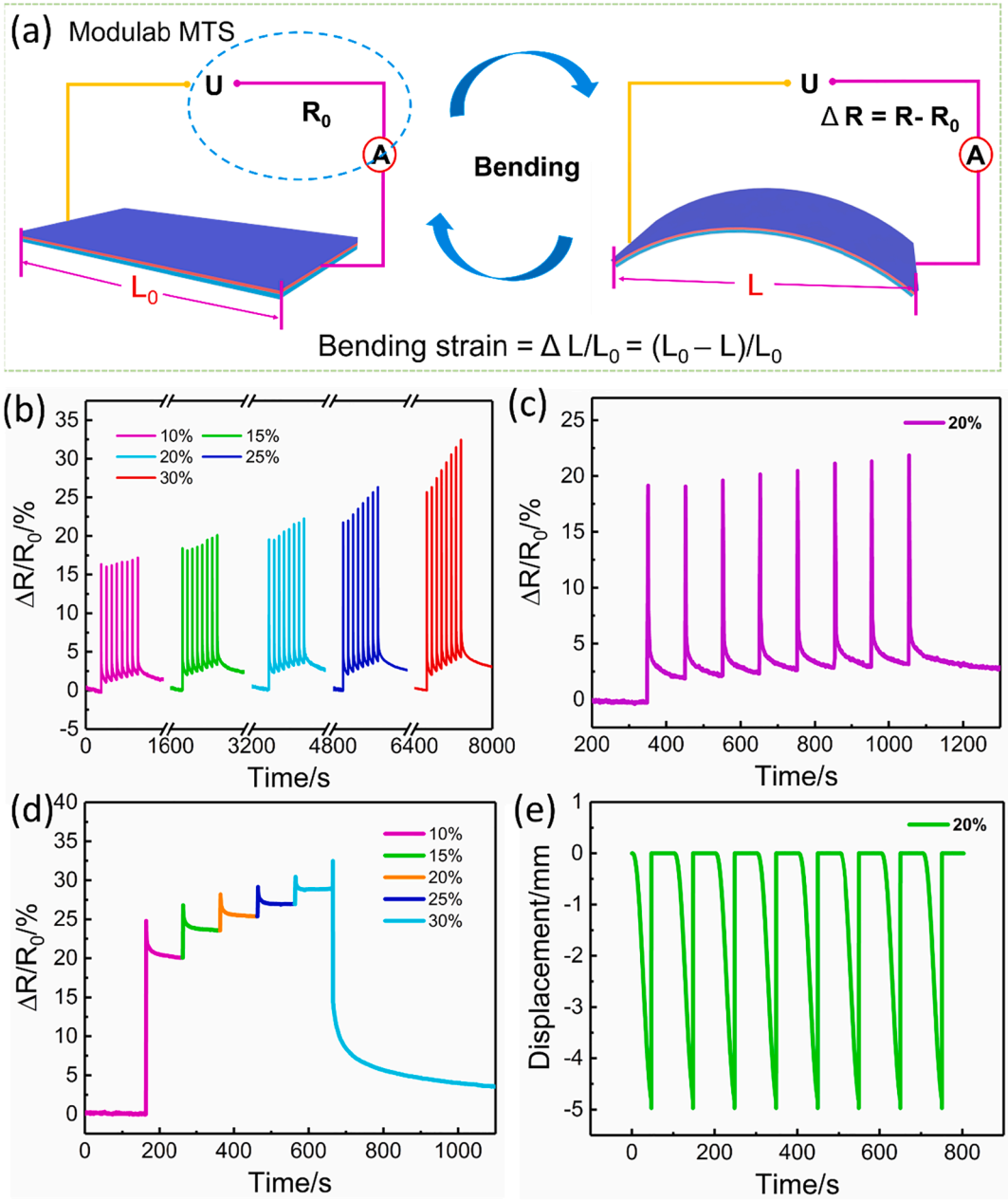


**Fig. 4.** (a) Schematic diagram of piezoresistive sensing using DMA measurement and impedance instrument. (b) Sensing signals ($\Delta R/R_0$ values) of PVDF/MXene/PI wearable electronic under different bending strain. (c) The $\Delta R/R_0$ values of PVDF/MXene/PI wearable electronic under 20% cyclic bending strain and (e) the corresponding bending displacement of PVDF/MXene/PI wearable electronic under 20% cyclic bending strain. (d) The $\Delta R/R_0$ values of PVDF/MXene/PI wearable electronic under step by step loading with increasing bending strain.

25% to 30% (Figure S4), the $\Delta R/R_0$ values increases from 17%, 20%, 23%, 26% to 32%, respectively. In Fig. 4b, the $\Delta R/R_0$ in different percentage bending strain is not stable. Since the as-fabricated PVDF/MXene/PI sensor is lab-grade product and not as stable as industrial grade products, it is difficult to accurately determine the external strain through a single measurement, so we hope that it can distinguish different strain by means of average value through multiple measurements. As shown in Figure S5, the mean value of the resistance change shows a stable and rising change with the increase of strain in multiple measurements, which shows the reliability of the measurement method and further indicates that the as-developed PVDF/MXene/PI sensor is capable to recognize different strain *via* the resistance change signal. Importantly, the $\Delta R/R_0$ values and the bending displacement both show good stability and cyclicity under 20% bending strain (Fig. 4c and e). Besides, the response performance under different forms of strain stimuli was also investigated. Fig. 4d explores the stimulus–response performance of PVDF/MXene/PI wearable sensor under continuous loading of different strains from 10% to 35% with an increment of 5% strain. By gradually loading different strains, the $\Delta R/R_0$ values of PVDF/MXene/PI wearable electronic presents a stepwise increase, further illustrating that PVDF/MXene/PI wearable electronic exhibits obvious mechanical–electrical sensing performance. In each stimulus–response stage, the dwell time is 100 s. When the PVDF/MXene/PI sensor is subjected to the corresponding strain, the resistance initially increases. Once the stimulation is over, the resistance of the sensor tends to the initial value, thus the resistance decreased and the curve sudden drops. Because the resistance of the PVDF/MXene/PI sensor needs a long time to recover, the resistance can only recover to a certain value within 100 s. When the strain is finally loaded to 30% and the stimulation ends, the resistance recovery time is long enough, so there is a very large drop of $\Delta R/R_0$ value from 32.5% to 2.5% in resistance. In conclusion, PVDF/MXene/PI is expected to be used in wearable electronic sensing devices to monitor different deformation.

### 3.3. *Multiple stimuli perception and body monitoring performance of PVDF/MXene/PI wearable electronic*

To study the human tactile perception behavior of PVDF/MXene/PI wearable electronic, various human movements and complex muscle movements were monitored respectively. When the finger gently touched the sample, PVDF/MXene/PI wearable electronic immediately generated a resistance-changed signal. After the finger was removed, the resistance value simultaneously recovered, exhibiting excellent human body monitoring behavior (Fig. 5a). Similarly, PVDF/MXene/PI wearable electronic can also generate different $\Delta R/R_0$ values under finger stroking and finger pressing due to difference in applied stress (Fig. 5b and c). Larger applied stress caused larger $\Delta R/R_0$ value, thus can sensitively distinguish different hand movements. Interestingly, it can

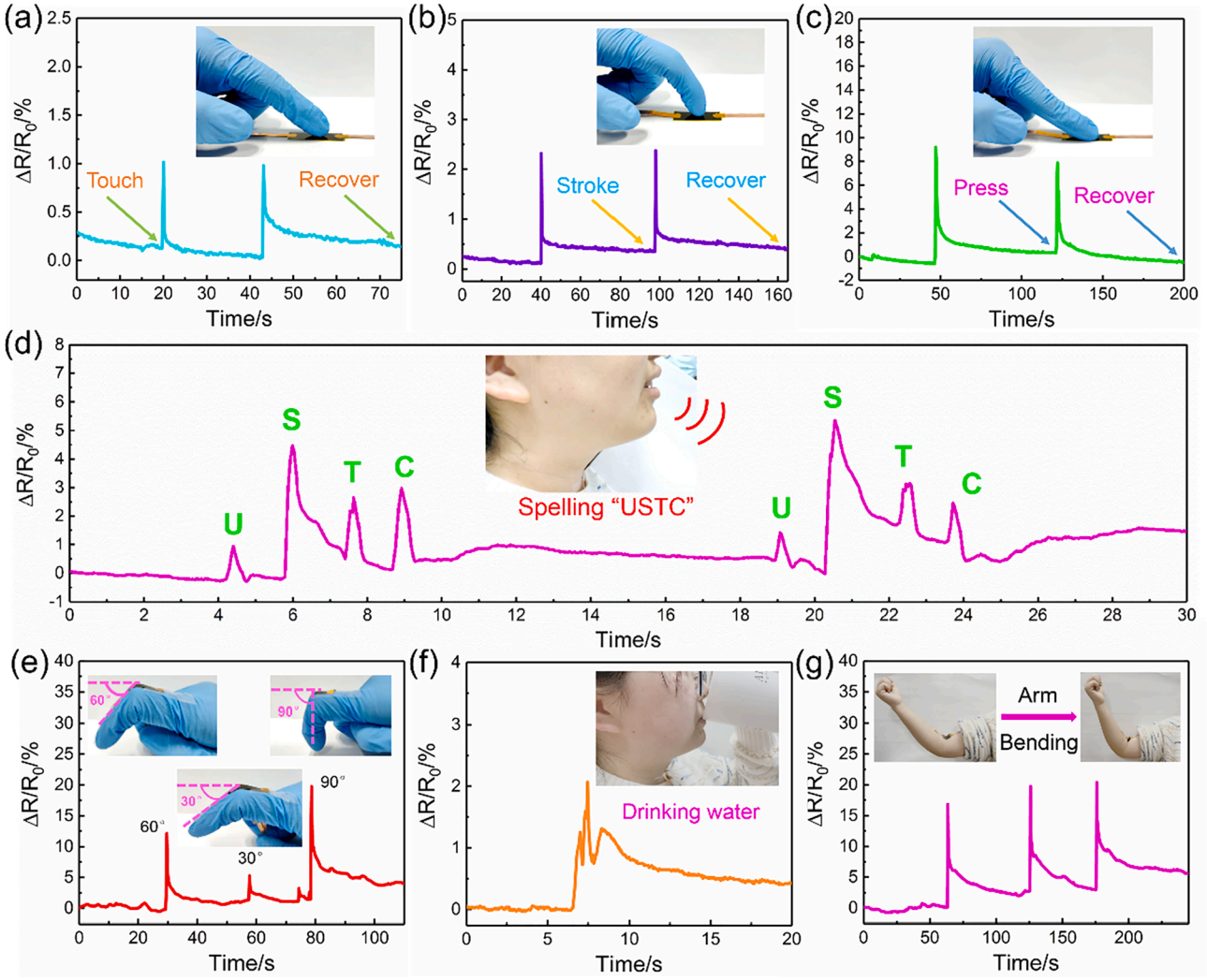


**Fig. 5.** The different $\Delta R/R_0$ values of PVDF/MXene/PI wearable electronic under different human movements, such as finger touching (a); finger stroking (b); finger pressing (c); speaking (d); finger bending (e); drinking water (f) and arm bending (g).

detect the movement of the larynx by spelling "University of Science and Technology of China (USTC)". As shown in Fig. 5d, when the throat reads the letter "USTC", four peaks of different shapes with different $\Delta R/R_0$ values appear, corresponding to "U", "S", "T" and "C". More importantly, the significant $\Delta R/R_0$ changes can also be used to distinguish the accent from the light tone, which shows the sensitivity of the PVDF/MXene/PI wearable electronic to perceive human behavior. Fig. 5e–g further shows a series of human monitoring properties of PVDF/MXene/PI wearable electronic, such as the bending of fingers at different angles, drinking water and bending of arms. Therefore, PVDF/MXene/PI wearable electronic possesses high sensitivity, excellent sensing performance and cyclic stability, thus shows potential application prospects in monitoring and analyzing human movement.

### 3.4. The Joule electrothermal performance of PVDF/MXene/PI wearable electronic

According to the Joule's law, the Joule heating performance of the

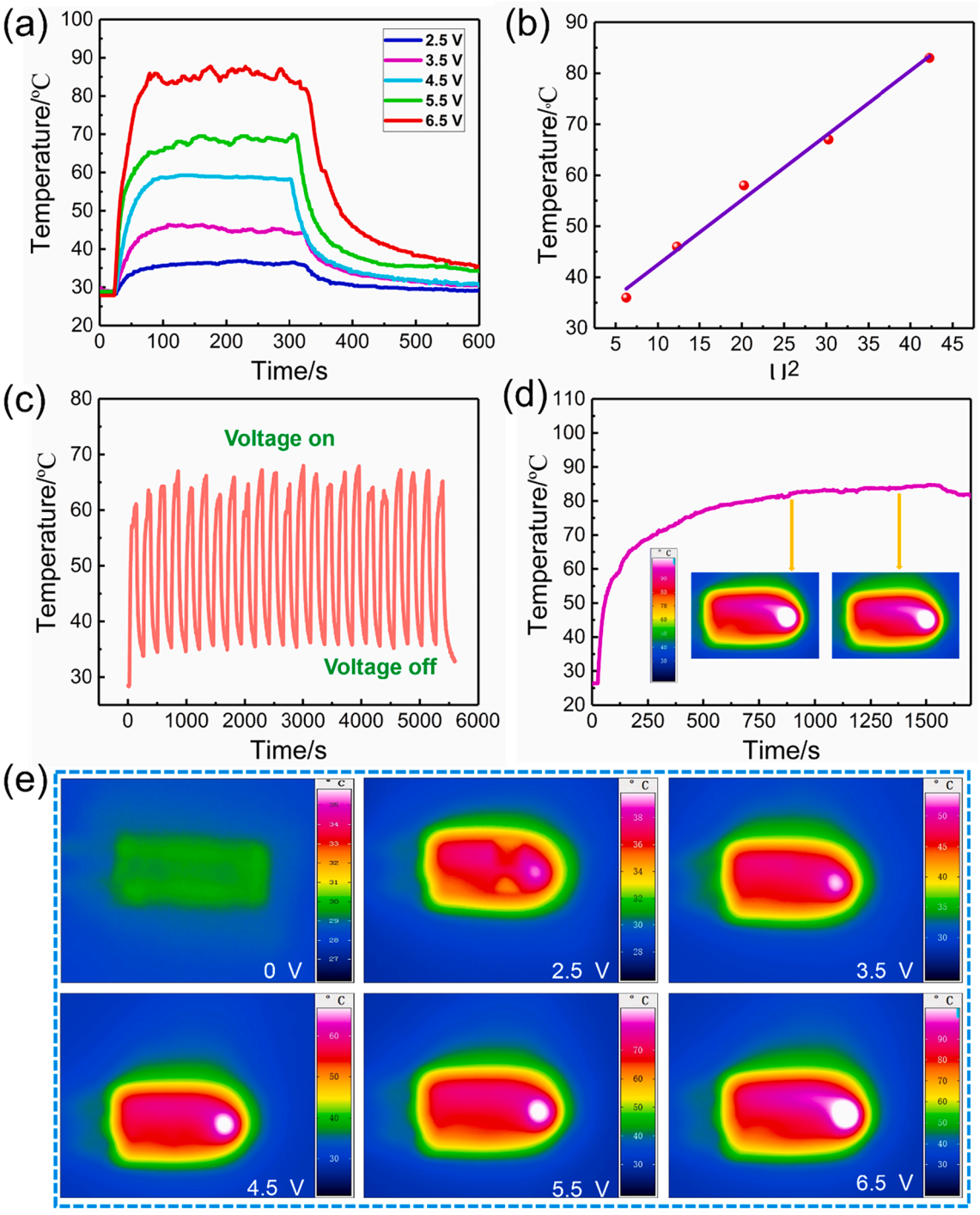


**Fig. 6.** (a) The temperature profile curves of PVDF/MXene/PI composite structure under different voltages. (b) The graph of the relationship between saturation temperature and voltage under different loading voltages. (c) The cyclic electric heating performance of PVDF/MXene/PI composite structure under 5.5 V loading voltage. (d) The temperature stability under the constant loading voltage of 6.5 V (inset pictures are the corresponding infrared thermal images). (e) The corresponding infrared thermal images of PVDF/MXene/PI heater under different voltages.

PVDF/MXene/PI wearable electronic under different loading voltages was studied. As shown in Fig. 6a, when the voltage increases from 2.5 V to 6.5 V, the maximum saturation temperature of PVDF/MXene/PI rises rapidly from 29 to 84 °C. The saturation temperature increases with the improvement of the input voltage, and shows a good linear relationship with the square of the voltage, indicating that the heat generated by PVDF/MXene/PI wearable electronic can be controlled by the external electrical power (Fig. 6b). Furthermore, the cyclic stability of the heating performance was investigated. In each cycle, the temperature first rises to the saturation temperature, and then drops to the initial temperature. During 23 heating cycles, PVDF/MXene/PI wearable electronic can still maintain its saturation temperature at about 62 °C when the applied voltage is 5.5 V, confirming its stable cyclic heating performance (Fig. 6c). In addition, the temperature change curve under 6.5 V constant voltage loading over 1800 long-time was also tested, further guarantees its long-term heating stability and durability (Fig. 6d). Furthermore, the corresponding infrared thermal images of PVDF/MXene/PI heater under different voltages also show the uniform distribution of temperature (Fig. 6e). Thus, the prepared PVDF/MXene/PI wearable electronic has good electric heating performance, and is expected to be used for the human heating and human thermal therapy.

### 3.5. The wearable electrical heating performance of PVDF/MXene/PI heater

The wearable heating behavior of PVDF/MXene/PI heater fixed on the back of hand demonstrates the activity of the electrical heater on the particular human body region (Fig. 7a–f). The wearable heater can warm up the specific hand surface to 39.3 ℃ and 55.4 ℃, whereas the rest of the other area without PVDF/MXene/PI electronic heater remains unaffected (Fig. 7a–c), indicating the viability of using PVDF/MXene/PI as a wearable heater to treat and relieve rheumatism and joint pain for human thermotherapy. Besides, the flexibility of PVDF/MXene/PI electronic heater guarantees the stable heat generation performance under the bending state (Fig. 7d–f). Furthermore, the wide temperature range make PVDF/MXene/PI electronic heater can be used to heat ice water and make the ice water melt (Fig. 7g). Therefore, PVDF/MXene/PI wearable heater shows promising prospects not only in electronic therapy and keeping warm for human beings, but also in heating and melting the ice water for human drinking. Finally, the insulating and high-temperature resistant PVDF and PI tapes are selected as the protective layer, not only preventing the conductive MXene layer from being directly exposed to the external environment, but also avoiding direct contact with the skin when used for human thermal treatment, ensuring the stability and safety of PVDF/MXene/PI wearable electronic as an electric heater.

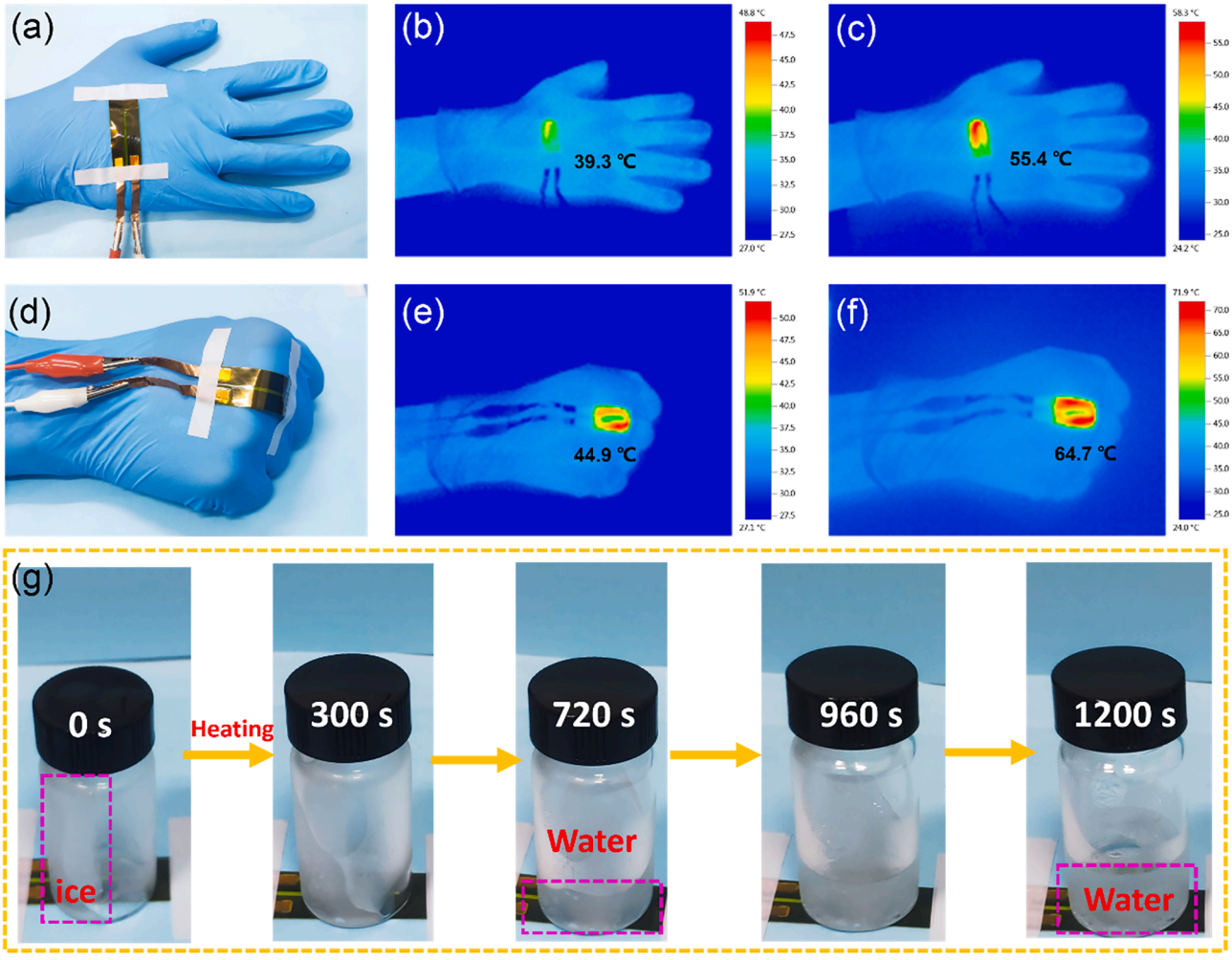


**Fig. 7.** (a) The digital image of PVDF/MXene/PI electronic heater attached on the back of hand. The IR images of the heater on the hand at the voltage of (b) 2.5 V and (c) 4.5 V. (d) The digital image of PVDF/MXene/PI electronic heater attached on the back of hand under the bending state. The IR images of the heater on the hand under the bending state at the voltage of (e) 3.5 V and (f) 5.5 V. (g) Digital images of the ice/water at different times during the melting process heated by PVDF/MXene/PI electronic heater.

### 3.6. The electrical conductivity and electromagnetic interference (EMI) shielding performance of PVDF/MXene/PI wearable electronic

According to the electromagnetic theory, the key to improve the electromagnetic shielding performance is to introduce conductive components so as to improve the electrical conductivity of materials. As shown in Fig. 8d, the electrical conductivity of PVDF/MXene composites was greatly improved after spray-coating the conductive MXene nanosheets. With the increase of MXene content, the electrical conductivity shows an increasing trend and the highest electrical conductivity can reach 4300 S/m. The excellent inherent conductivity of MXene enables PVDF/MXene/PI wearable electronic to exhibit superior electromagnetic shielding performance. To evaluate the electromagnetic shielding performance of PVDF/MXene/PI wearable electronic, the EMI SE values in the frequency range of 8.2–12.4 GHz (X-band) were tested. As shown in Fig. 8a, PVDF and PI tapes have almost no electromagnetic shielding ability. By spraying conductive MXene on the PVDF film surface with the MXene surface density of 0.035 mg/cm$^2$, the electromagnetic shielding value can be effectively increased to 21 dB. As the amount of MXene increases, the EMI SE value of the PVDF/MXene/PI wearable electronic also gradually increases. When the spraying amount of MXene reaches 0.165 mg/cm$^2$, the electromagnetic shielding value of PVDF/MXene/PI can reach 40 dB, indicating PVDF/MXene/PI can availably block the electromagnetic radiation and protect the human body.

To understand the electromagnetic shielding mechanism [32], the contribution of reflection ($SE_R$) and absorption ($SE_A$) to the total electromagnetic shielding effectiveness ($SE_T$) were calculated in Fig. 8b. Obviously, the $SE_R$, $SE_A$ and $SE_T$ values are all increased with the increase of MXene amount. The $SE_A$ value is always higher than the $SE_R$ value, suggesting that both the reflection and absorption mechanisms contribute to the EMI shielding ability. In order to further determine the main mechanism of shielding electromagnetic waves for PVDF/MXene/

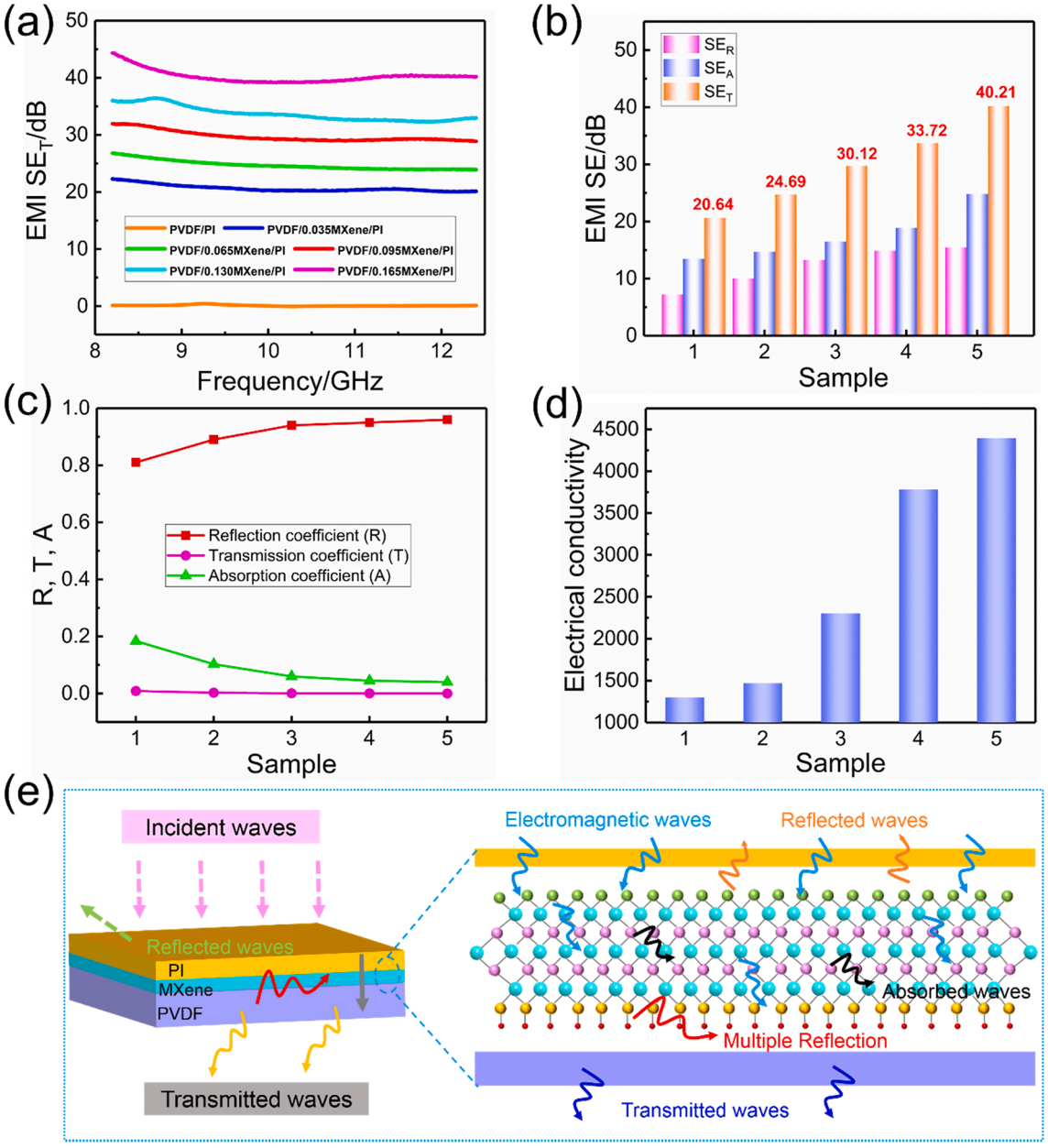


**Fig. 8.** (a) EMI shielding values, (b) average EMI $SE_T$, $SE_A$ and $SE_R$ values (sample 1–5 refer to PVDF/0.035MXene/PI, PVDF/0.065MXene/PI, PVDF/0.095MXene/PI, PVDF/0.130MXene/PI and PVDF/0.165MXene/PI, respectively), (c) R, A and T coefficients and (d) electrical conductivity of PVDF/MXene/PI wearable with different MXene contents. (e) Schematic illustration of EMI shielding mechanism for PVDF/MXene/PI wearable electronic.

PI wearable electronic, the R, A and T coefficients are calculated. As the content of MXene increases, the R value shows an increasing trend, while the A value shows a downward trend (Fig. 8c). Moreover, the R value is much higher than the A value, indicating PVDF/MXene/PI wearable electronic mainly shields electromagnetic waves by reflecting electromagnetic radiation. In addition, the extremely small T value states that the incident electromagnetic waves are basically shielded, further confirms the remarkable EMI shielding behavior of PVDF/MXene/PI wearable electronic. Here, the EMI shielding performance of other previously reported composites are consulted in Table S1. It is found that the PVDF/MXene/PI composite structure shows an excellent EMI shielding ability compared with these similar composites [33-39].

Fig. 8e shows the spreading process of electromagnetic waves through the PVDF/MXene/PI wearable electronic and possible shielding mechanism in detail. Since PVDF and PI tapes are completely transparent to electromagnetic waves, the incident electromagnetic waves collide with the surface of MXene layer. Due to the impedance mismatch of the MXene-air interface, a large part of the electromagnetic wave is reflected firstly. The remaining electromagnetic waves then enter into the layered structure of MXene and interacts with the high charge density of MXene, causing ohmic loss and leading a significant absorption of the electromagnetic waves. In addition, the layered structure of MXene nanosheets is conducive to the multiple reflection of electromagnetic waves, which can effectively expedite the conversion of electromagnetic waves into heat loss, thus enhancing the absorption and attenuation of incident electromagnetic waves. Moreover, the functional groups (–OH, -F, -O, etc) and Ti in MXene will cause dipolar polarization loss when contacts electromagnetic waves, further dissipating electromagnetic waves and improving the total shielding effectiveness.

## 4. Conclusions

In summary, a multifunctional PVDF/MXene/PI wearable electronic was constructed by spray-coating the conductive MXene nanosheets on the PVDF film and followed by assembling the PI tape. Through assembling, PVDF/MXene/PI composite structure is not only endowed with ideal versatility, but also is able to maintain good toughness and mechanical strength. By forming the conductive MXene layer, the resistance of PVDF/MXene/PI changes under the stimulation of external strain, thus can respond to the different strain. Moreover, PVDF/MXene/PI wearable electronic can monitor different human muscle movements such as finger bending, arm bending, drinking water and talking, which shows good monitoring sensitivity and cyclicality. Based on the Joule heating effect, the conductive layer MXene in the PVDF/MXene/PI wearable electronic can generate heat under the loading of voltage, thus can be used as a heater to provide electrical therapy for the human body. Interestingly, the conductive MXene network improves the electromagnetic shielding performance of PVDF/MXene/PI wearable electronic with the maximum $SE_T$ of 40 dB, thus provides electromagnetic protection for the human body. In conclusion, this multifunctional PVDF/MXene/PI wearable electronic shows expansive application values in the field of wearable electronic devices and human body protection.

## CRediT authorship contribution statement

**Min Sang:** Investigation, Writing – original draft, Methodology, Visualization. **Shuai Liu:** Investigation, Writing – original draft, Formal analysis. **Wenwen Li:** Investigation, Writing – original draft, Formal analysis. **Sheng Wang:** Formal analysis, Writing – review & editing, Data curation. **Jun Li:** Investigation, Methodology, Data curation. **Ji Li:** Investigation, Methodology, Data curation. **Shouhu Xuan:** Methodology, Investigation, Writing – review & editing. **Xinglong Gong:** Resources, Supervision, Project administration, Funding acquisition.

## Declaration of Competing Interest

The authors declare that they have no known competing financial interests or personal relationships that could have appeared to influence the work reported in this paper.

## Acknowledgements

Financial supports from the National Natural Science Foundation of China (Grant Nos. 11822209, 11972032, 12072338, 12132016), the Fundamental Research Funds for the Central Universities (WK2480000007), the Joint Fund of USTC-National Synchrotron Radiation Laboratory (KY2090000055) and the Anhui's Key R&D Program of China (202104a05020009) are gratefully acknowledged.

## Appendix A. Supplementary material

Supplementary data to this article can be found online at https://doi.org/10.1016/j.compositesa.2021.106727.

## References

[1] Li Z, Liu P, Ji X, Gong J, Hu Y, Wu W, et al. Bioinspired simultaneous changes in fluorescence color, brightness, and shape of hydrogels enabled by AIEgens. Adv. Mater. 2020;32(11):1906493. https://doi.org/10.1002/adma.201906493.
[2] Stadlober B, Zirkl M, Irimia-Vladu M. Route towards sustainable smart sensors: ferroelectric polyvinylidene fluoride-based materials and their integration in flexible electronics. Chem. Soc. Rev. 2019;48(6):1787–825.
[3] Xie X, Huang H, Zhu J, Yu J, Wang Y, Hu Z. A spirally layered carbon nanotube graphene/polyurethane composite yarn for highly sensitive and stretchable strain sensor. Compos. Part A-Appl. S 2020;135:105932. https://doi.org/10.1016/j.compositesa:2020.105932.
[4] Maiti S, Karan SK, Kim JK, Khatua BB. Nature driven bio-piezoelectric/triboelectric nanogenerator as next-generation green energy harvester for smart and pollution free society. Adv. Energy Mater. 2019;9(9):1803027. https://doi.org/10.1002/aenm.201803027.
[5] Mondal S, Kim SJ, Choi C-G. Honeycomb-like $MoS_2$ nanotube array-based wearable sensors for noninvasive detection of human skin moisture. ACS Appl. Mater. Interfaces 2020;12(14):17029–38.
[6] Zhang P, Gao Di, An K, Shen Qi, Wang C, Zhang Y, et al. A programmable polymer library that enables the construction of stimuli-responsive nanocarriers containing logic gates. Nat. Chem. 2020;12(4):381–90.
[7] Salaeh S, Das A, Stöckelhuber KW, Wießner S. Fabrication of a strain sensor from a thermoplastic vulcanizate with an embedded interconnected conducting filler network. Compos. Part A-Appl. S 2020;130:105763. https://doi.org/10.1016/j.compositesa:2020.105763.
[8] Ma Y, Yao J, Liu Q, Han T, Zhao J, Ma X, et al. Liquid bandage harvests robust adhesive, hemostatic and antibacterial performances as a first-aid tissue adhesive. Adv. Funct. Mater. 2020;30(39):2001820. https://doi.org/10.1002/adfm.202001820.
[9] Yao B, Hong W, Chen T, Han Z, Xu X, Hu R, et al. Highly stretchable polymer composite with strain-enhanced electromagnetic interference shielding effectiveness. Adv. Mater. 2020;32(14):1907499. https://doi.org/10.1002/adma.201907499.
[10] Stam R, Yamaguchi-Sekino S. Occupational exposure to electromagnetic fields from medical sources. Ind. Health 2018;56(2):96–105.
[11] Ghosh S, Nitin B, Remanan S, Bhattacharjee Y, Ghorai A, Dey T, et al. A multifunctional smart textile derived from merino wool/nylon polymer nanocomposites as next generation microwave absorber and soft touch sensor. ACS Appl. Mater. Interfaces 2020;12(15):17988–8001.
[12] Yin Y, Cui Y, Li Y, Xing Y, Li M. Thermal management of flexible wearable electronic devices integrated with human skin considering clothing effect. Appl. Therm. Eng. 2018;144:504–11.
[13] Ma Z, Kang S, Ma J, Shao L, Wei A, Liang C, et al. High-performance and rapid-response electrical heaters based on ultra-flexible, heat-resistant, and mechanically strong aramid nanofiber/Ag nanowire nanocomposite papers. ACS Nano 2019;13(7):7578–90.
[14] Qiu K, Elhassan A, Tian T, Yin X, Yu J, Li Z, et al. Highly flexible, efficient, and sandwich-structured infrared radiation heating fabric. ACS Appl. Mater. Interfaces 2020;12(9):11016–25.
[15] Xu F, Aouraghe MA, Xie X, Zheng L, Zhang K, Fu KK. Highly stretchable, fast thermal response carbon nanotube composite heater. Compos. Part A-Appl. S 2021;147:106471. https://doi.org/10.1016/j.compositesa:2021.106471.
[16] Liu Q, Tian B, Luo C, Liang J, Wu W. Printed flexible heaters-based thermotherapy platform for multiduty thermal management. Adv. Mater. Technol. 2020;5(8):2000278. https://doi.org/10.1002/admt.202000278.
[17] Wang Z, Cheng Z, Fang C, Hou X, Xie Li. Recent advances in MXenes composites for electromagnetic interference shielding and microwave absorption. Compos. Part A-Appl. S 2020;136:105956. https://doi.org/10.1016/j.compositesa:2020.105956.

[18] Shahzad F, Alhabeb M, Hatter CB, Anasori B, Man Hong S, Koo CM, et al. Electromagnetic interference shielding with 2D transition metal carbides (MXenes). Science 2016;353(6304):1137–40.
[19] Levitt A, Zhang J, Dion G, Gogotsi Y, Razal JM. MXene-based fibers, yarns, and fabrics for wearable energy storage devices. Adv. Funct. Mater. 2020;30(47): 2000739. https://doi.org/10.1002/adfm.202000739.
[20] Sarycheva A, Polemi A, Liu Y, Dandekar K, Anasori B, Gogotsi Y. 2D titanium carbide (MXene) for wireless communication. Sci. Adv. 2018;4(9). https://doi.org/10.1126/sciadv.aau0920.
[21] Zhou B, Li Z, Li Y, Liu X, Ma J, Feng Y, et al. Flexible hydrophobic 2D $Ti_3C_2Tx$-based transparent conductive film with multifunctional self-cleaning, electromagnetic interference shielding and joule heating capacities. Compos. Sci. Technol. 2021;201:108531. https://doi.org/10.1016/j.compscitech.2020.108531.
[22] Li K, Chang T-H, Li Z, Yang H, Fu F, Li T, et al. Biomimetic MXene textures with enhanced light-to-heat conversion for solar steam generation and wearable thermal management. Adv. Energy Mater. 2019;9(34):1901687. https://doi.org/10.1002/aenm.201901687.
[23] Fu Z, Wang N, Legut D, Si C, Zhang Q, Du S, et al. Rational design of flexible two-dimensional MXenes with multiple functionalities. Chem. Rev. 2019;119(23): 11980–2031.
[24] Anasori B, Lukatskaya MR, Gogotsi Y. 2D metal carbides and nitrides (MXenes) for energy storage. Nat. Rev. Mater. 2017;2:16098.
[25] Chen W, Liu L-X, Zhang H-B, Yu Z-Z. Kirigami-inspired highly stretchable, conductive, and hierarchical $Ti_3C_2Tx$ MXene films for efficient electromagnetic interference shielding and pressure sensing. ACS Nano 2021;15(4):7668–81.
[26] Liu X, Jin X, Li L, Wang J, Yang Y, Cao Y, et al. Air-permeable, multifunctional, dual-energy driven MXene-decorated polymeric textile-based wearable heaters with exceptional electrothermal and photothermal conversion performance. J. Mater. Chem. A 2020;8(25):12526–37.
[27] Wang J, Liu Y, Cheng Z, Xie Z, Yin L, Wang Wu, et al. Highly conductive MXene film actuator based on moisture gradients. Angew. Chem. Int. Ed. 2020;59(33): 14029–33.
[28] Li S, Wang J, Zhu Z, Liu D, Li W, Sui G, et al. CVD carbon-coated carbonized loofah sponge loaded with a directionally arrayed MXene aerogel for electromagnetic interference shielding. J. Mater. Chem. A 2021;9(1):358–70.
[29] Sang M, Wang S, Liu M, Bai L, Jiang W, Xuan S, et al. Fabrication of a piezoelectric polyvinylidene fluoride/carbonyl iron (PVDF/CI) magnetic composite film towards the magnetic field and deformation bi-sensor. Compos. Sci. Technol. 2018;165: 31–8.
[30] Zhu L, Dikin DA, Percec S, Ren F. Improving interlayer adhesion of poly(p-phenylene terephthalamide) (PPTA)/ultra-high-molecular-weight polyethylene (UHMWPE) laminates prepared by plasma treatment and hot pressing technique. Polymers 2021;13(16):2600. https://doi.org/10.3390/polym13162600.
[31] Li Y, Xin B, Lu Z, Zhou X, Liu Y, Hu Y. Enhancing the supercapacitor performance of flexible MXene/carbon cloth electrodes by oxygen plasma and chemistry modification. Int. J. Energy Res. 2021;45:9229–40.
[32] Pei X, Zhao M, Li R, Lu H, Yu R, Xu Z, et al. Porous network carbon nanotubes/chitosan 3D printed composites based on ball milling for electromagnetic shielding. Compos. Part A-Appl. S 2021;145:106363. https://doi.org/10.1016/j.compositesa:2021.106363.
[33] Hu Y, Tang P, Li L, Yang J, Jian X, Bin Y. High absorption shielding material of poly (phthalazinone etherketone)/multiwall carbon nanotube composite films with sandwich configurations. RSC Adv. 2019;9(33):18758–66.
[34] Fei Y, Liang M, Chen Y, Zou H. Sandwich-like magnetic graphene papers prepared with MOF derived $Fe_3O_4$-C for absorption-dominated electromagnetic interference shielding. Ind. Eng. Chem. Res. 2020;59(1):154–65.
[35] Xie Q, Yan Z, Wang S, Wang Y, Mei L, Qin F, et al. Transparent, flexible, and stable polyethersulfone/copper-nanowires/polyethylene terephthalate sandwich-structured films for high-performance electromagnetic interference shielding. Adv. Eng. Mater. 2021;23:2100283.
[36] Hu M, Gao J, Dong Y, Li K, Shan G, Yang S, et al. Flexible transparent PES/silver nanowires/PET sandwich-structured film for high-efficiency electromagnetic interference shielding. Langmuir 2012;28:7101–6.
[37] Kumar P, Shahzad F, Hongac S, Koo C. A flexible sandwich graphene/silver nanowires/graphene thin film for high-performance electromagnetic interference shielding. RSC Adv. 2016;6:101283–7.
[38] Zhang Y, Ruan K, Gu J. Flexible sandwich-structured electromagnetic interference shielding nanocomposite films with excellent thermal conductivities. Small 2021; 2101951.
[39] Zhu X, Guo A, Yan Z, Qin F, Xu J, Ji Y, et al. PET/Ag NW/PMMA transparent electromagnetic interference shielding films with high stability and flexibility. Nanoscale 2021;13:8067–76.